

Selectively Targeting Tumor Hypoxia With the Hypoxia-Activated Prodrug CP-506



Alexander M.A. van der Wiel¹, Victoria Jackson-Patel^{2,3}, Raymon Niemans¹, Ala Yaromina¹, Emily Liu², Damiënne Marcus¹, Alexandra M. Mowday^{1,2}, Natasja G. Lieuwes¹, Rianne Biemans¹, Xiaojing Lin^{2,3}, Zhe Fu^{2,3}, Sisira Kumara^{2,3}, Arthur Jochems¹, Amir Ashoorzadeh^{2,3}, Robert F. Anderson^{2,3}, Kevin O. Hicks^{2,3}, Matthew R. Bull^{2,3}, Maria R. Abbattista^{2,3}, Christopher P. Guise^{2,3}, Sofie Deschoemaeker⁴, Sophie Thiolloy⁴, Arne Heyerick⁴, Morwena J. Solivio⁵, Silvia Balbo⁵, Jeff B. Smail^{2,3}, Jan Theys¹, Ludwig J. Dubois¹, Adam V. Patterson^{2,3}, and Philippe Lambin¹

ABSTRACT

Hypoxia-activated prodrugs (HAP) are a promising class of antineoplastic agents that can selectively eliminate hypoxic tumor cells. This study evaluates the hypoxia-selectivity and antitumor activity of CP-506, a DNA alkylating HAP with favorable pharmacologic properties. Stoichiometry of reduction, one-electron affinity, and back-oxidation rate of CP-506 were characterized by fast-reaction radiolytic methods with observed parameters fulfilling requirements for oxygen-sensitive bioactivation. Net reduction, metabolism, and cytotoxicity of CP-506 were maximally inhibited at oxygen concentrations above 1 $\mu\text{mol/L}$ (0.1% O_2). CP-506 demonstrated cytotoxicity selectively in hypoxic 2D and 3D cell cultures with normoxic/anoxic IC_{50} ratios up to 203. Complete resistance to aerobic (two-electron) metabolism by aldo-keto reduc-

tase 1C3 was confirmed through gain-of-function studies while retention of hypoxic (one-electron) bioactivation by various diflavin oxidoreductases was also demonstrated. *In vivo*, the antitumor effects of CP-506 were selective for hypoxic tumor cells and causally related to tumor oxygenation. CP-506 effectively decreased the hypoxic fraction and inhibited growth of a wide range of hypoxic xenografts. A multivariate regression analysis revealed baseline tumor hypoxia and *in vitro* sensitivity to CP-506 were significantly correlated with treatment response. Our results demonstrate that CP-506 selectively targets hypoxic tumor cells and has broad antitumor activity. Our data indicate that tumor hypoxia and cellular sensitivity to CP-506 are strong determinants of the antitumor effects of CP-506.

Introduction

Hypoxia is a common feature in the majority of solid tumors that arises due to a disruption of the balance between proliferation and oxygen supply (1). Given its pivotal role in tumor progression and resistance to conventional therapies (2), several strategies have been developed to overcome tumor hypoxia, including the use of hypoxia-activated prodrugs (HAPs; ref. 3). HAPs are low-molecular weight

therapeutic agents that, only under sufficiently low oxygen tension, are bioactivated by enzymatic reduction to typically generate cytotoxic effector molecules (4).

Six HAPs have previously been evaluated in a clinical setting (5, 6). Evofosfamide (TH-302), a 2-nitroimidazole-based phosphoramidate mustard HAP, demonstrated single-agent antitumor activity (7) that is further increased when combined with conventional anticancer therapies, both preclinically (8–10) and clinically (11, 12). However, addition of evofosfamide to standard of care treatment failed to improve overall survival in pancreatic cancer (NCT01746979; ref. 13) and soft tissue carcinoma (NCT01440088; ref. 14). Potential explanations are a lack of patient stratification (3), unexpected lowering of pharmacokinetic exposures due to prodrug reformulation during the phase III trials (15), and limited diffusion of its cytotoxic metabolite (bystander effect; refs. 16, 17). PR-104, a phosphate pre-prodrug of the dinitrobenzamide nitrogen mustard HAP PR-104A, demonstrated hypoxia-selective activation *in vitro* (PR-104A) and *in vivo* (PR-104; ref. 18). The combination of PR-104 with radio- or chemotherapy further enhanced its antitumor effects (18–20). However, clinical safety and tolerability of PR-104 demonstrated dose-limiting thrombocytopenia and neutropenia (21, 22). Subsequent preclinical studies elucidated that PR-104A can be activated independent of tissue oxygenation by human two-electron aldo-keto reductase 1C3 (AKR1C3; refs. 23, 24). Further clinical evaluation revealed that myelotoxicity was the only serious adverse event preventing dose-escalation of PR-104 administration (25) and reaching adequate plasma concentrations for monotherapeutic efficacy (21, 22, 26). Hence, avoiding AKR1C3 bioactivation should suppress prodrug myelotoxicity and permit significant dose-escalation without encountering treatment-related hematologic adverse effects.

¹The D-Lab and The M-Lab, Department of Precision Medicine, GROW – School for Oncology and Developmental Biology, Maastricht University, Maastricht, the Netherlands. ²Auckland Cancer Society Research Centre, School of Medical Sciences, University of Auckland, Auckland, New Zealand. ³Maurice Wilkins Centre for Molecular Biodiscovery, University of Auckland, Auckland, New Zealand. ⁴Convert Pharmaceuticals, Liège, Belgium. ⁵Masonic Cancer Center, University of Minnesota, Minneapolis, Minnesota.

Note: Supplementary data for this article are available at Molecular Cancer Therapeutics Online (<http://mct.aacrjournals.org/>).

A.M.A. van der Wiel, V. Jackson-Patel, and R. Niemans contributed equally in this article.

L.J. Dubois, A.V. Patterson, and P. Lambin contributed equally as the co-senior authors of this article.

Corresponding Author: Adam V. Patterson, Auckland Cancer Society Research Centre, University of Auckland, Faculty of Medicine and Health Sciences, Auckland 1142, New Zealand. E-mail: a.patterson@auckland.ac.nz

Mol Cancer Ther 2021;20:2372–83

doi: 10.1158/1535-7163.MCT-21-0406

This open access article is distributed under Creative Commons Attribution-NonCommercial-NoDerivatives License 4.0 International (CC BY-NC-ND).

©2021 The Authors; Published by the American Association for Cancer Research

On the basis of this rationale, PR-104 was redesigned to give rise to CP-506, a next-generation HAP with more favorable properties (27–29). First, CP-506 is designed to be resistant to AKR1C3 metabolism, ensuring highly specific hypoxia-dependent activation. Second, CP-506 is a water-soluble piperazine mesylate salt, avoiding the need for a phosphate solubilization strategy utilized for PR-104, and is thus resistant to glucuronidation of the alcohol present in PR-104A, a major clearance pathway compromising its pharmacokinetic profile (30, 31). Third, CP-506 mesylate has the potential to be orally bioavailable. Fourth, CP-506 is a mono-nitro HAP, thereby avoiding facile metabolic loss via self-alkylation of the reduced nitro-group ortho to the mustard (18). Finally, physicochemical properties of CP-506 and its metabolites readily permit a bystander effect. The proposed mechanism of action of CP-506 (Fig. 1A) is similar to that of PR-104 (Supplementary Fig. S1).

In this study, we first characterized the stoichiometry of CP-506 reduction, one-electron affinity, and back-oxidation rate by using fast-reaction radiolytic methods. We accurately assessed the oxygen-dependence of CP-506 metabolism and cytotoxicity, evaluated resistance to aerobic AKR1C3 metabolism and the hypoxia-selective cytotoxicity and DNA adduct formation of CP-506 in a wide range of 2D and 3D *in vitro* models. *In vivo*, we first assessed whether a causal relationship existed between CP-506 efficacy and tumor oxygenation. We further characterized the antitumor effects of CP-506 in a broad panel of 15 human xenograft models. We hypothesized that CP-506 is effective in inhibiting growth of hypoxic tumors only, reducing their hypoxic fraction (HF). Finally, a multivariate linear regression analysis was performed to identify which factors ultimately contribute to CP-506 antitumor efficacy.

Materials and Methods

Compounds

CP-506 (2-[(2-bromoethyl)-5-[(4-ethyl-1-piperazinyl)carbonyl]-2-(methylsulfonyl)-4-nitroanilino]ethyl methanesulfonate), CP-506H (2-[(2-bromoethyl)-5-(4-ethylpiperazine-1-carbonyl)-4-(hydroxyamino)-2-(methylsulfonyl)phenyl]amino)ethyl methanesulfonate, and CP-506M (2-[(4-amino-5-(4-ethylpiperazine-1-carbonyl)-2-(methylsulfonyl)phenyl)(2-bromoethyl)amino]ethyl methanesulfonate) were manufactured by Mercachem employing synthetic routes developed at the University of Auckland (Supplementary Materials and Methods). Deuterated internal standards were prepared using identical synthetic procedures employing D8-1-ethylpiperazine instead of 1-ethylpiperazine. SN35393 (5-(bis(2-bromoethyl)amino)-4-(methylsulfonyl)-2-nitrophenyl)(4-methylpiperazin-1-yl)methanone) was synthesized as described previously (27). PR-104 was supplied by Proacta Inc. PR-104A was synthesized and purified as reported previously (32, 33). For *in vitro* experiments, stock solutions were made in dimethyl sulfoxide (DMSO) and stored at -20°C . For *in vivo* experiments, compounds were dissolved in water for injection (WFI).

Pulse and steady-state radiolysis studies

The one-electron reduction potential of CP-506 [$E^{\circ}(\text{S/S}^{-})$] was determined by a previously described pulse radiolysis method (34). UV-visible spectrum of the radical anion was produced by directly scavenging the radiolytically produced e_{aq}^{-} and by electron transfer from the CO_2^{-} radical. The back-oxidation rates of the radical anion were followed by time-resolved spectrophotometry with increasing concentrations of dissolved oxygen from which the second-order rate constant was determined. The stepwise reduction of CP-506 was followed using spectrophotometry by the addition of reducing equiva-

lents in anoxia produced upon steady-state radiolysis using a γ -ray ^{137}Cs source.

Cell culture

Cells were routinely cultured at 37°C in a humidified 5% CO_2 air atmosphere and were STR-authenticated and confirmed to be mycoplasma-free by PCR (Roche Diagnostics). Cells were routinely cultured for ≤ 10 weeks. Tissue of origin, provider, and culture medium of the employed cell lines are summarized in Supplementary Table S1. HCT116 cells overexpressing the human aldo-keto reductases 1C family members and human diflavin reductases were described previously (23, 35).

Assessment of oxygen-dependence of CP-506 activation

Stirred suspensions of HCT116 cells overexpressing cytochrome P450 oxidoreductase (POR; HCT116^{POR}) were exposed to variable gas mixtures (0%–95% O_2 , 5% CO_2 , residual N_2). After pre-equilibration, cell suspensions were treated with CP-506 (100 $\mu\text{mol/L}$, 1 h). Soluble (aqueous) oxygen concentrations were measured directly using a calibrated FOSPOR fiber-optic oxygen probe (Oxygen Optics). For metabolic endpoint, samples were crashed in acetonitrile containing deuterated internal standards and stored (-80°C) until LC/MS-MS analysis. For cell survival endpoint, samples were harvested and clonogenic survival was assessed after 12 days. Colonies (>50 cells) were manually counted to determine plating efficiency (PE). A linear regression between CP-506H formation or PE and CP-506 AUC was fitted and the KO_2 value, defined as the O_2 concentration required to reduce the effect of CP-506 to 50% of that effect in anoxic culture, was assessed.

Cell viability assays

Culture medium, 96-well plates, and pipet tips were preincubated 72 hours before use in normoxic or anoxic conditions in respectively a cell culture incubator (HERAccl 150 CO_2 Incubator; 21% O_2 , 5% CO_2) or anoxic workstations (A35 Don Whitley, Don Whitley Scientific; Bactron II, Shell Lab; <1 ppm O_2 , 10% H_2 , 5% CO_2 , residual N_2). Cells were transferred to normoxic or anoxic conditions and resuspended in preincubated medium. Cells were seeded in 96-well plates in optimized densities and were allowed to attach for 2 hours. CP-506 was dissolved in preincubated medium and cells were exposed to CP-506-containing medium for 4 hours. After, plates were transferred to normoxia, washed, and received fresh culture medium. Cell viability was assessed 96 hours after the start of treatment using the CellTiter-Glo 2.0 reagent (Promega) or 72 hours after the start of treatment using the alamarBlue reagent (Thermo Fisher) according to the manufacturer's protocol. Treatment response was quantified as IC_{50} , that is, the concentration of CP-506 that reduced cell viability by 50%. The hypoxia cytotoxicity ratio (HCR) was defined as the ratio of the normoxic to anoxic IC_{50} .

Multicellular layer clonogenic cell survival assay

Multicellular layers (MCL) were grown as described previously (36). MCLs were exposed to CP-506 for 5 hours under anoxic or hyperoxic (95% O_2 , 5% CO_2) conditions. MCLs were trypsinized and clonogenic survival was assessed after 10 days. Treatment response was quantified as IC_{10} , that is, the concentration of CP-506 resulting in 90% clonogenic cell kill.

Adductomics analyses

The LC/MS approach used for the identification and relative quantification of CP-506-induced DNA adduct formation is described in Supplementary Materials and Methods.

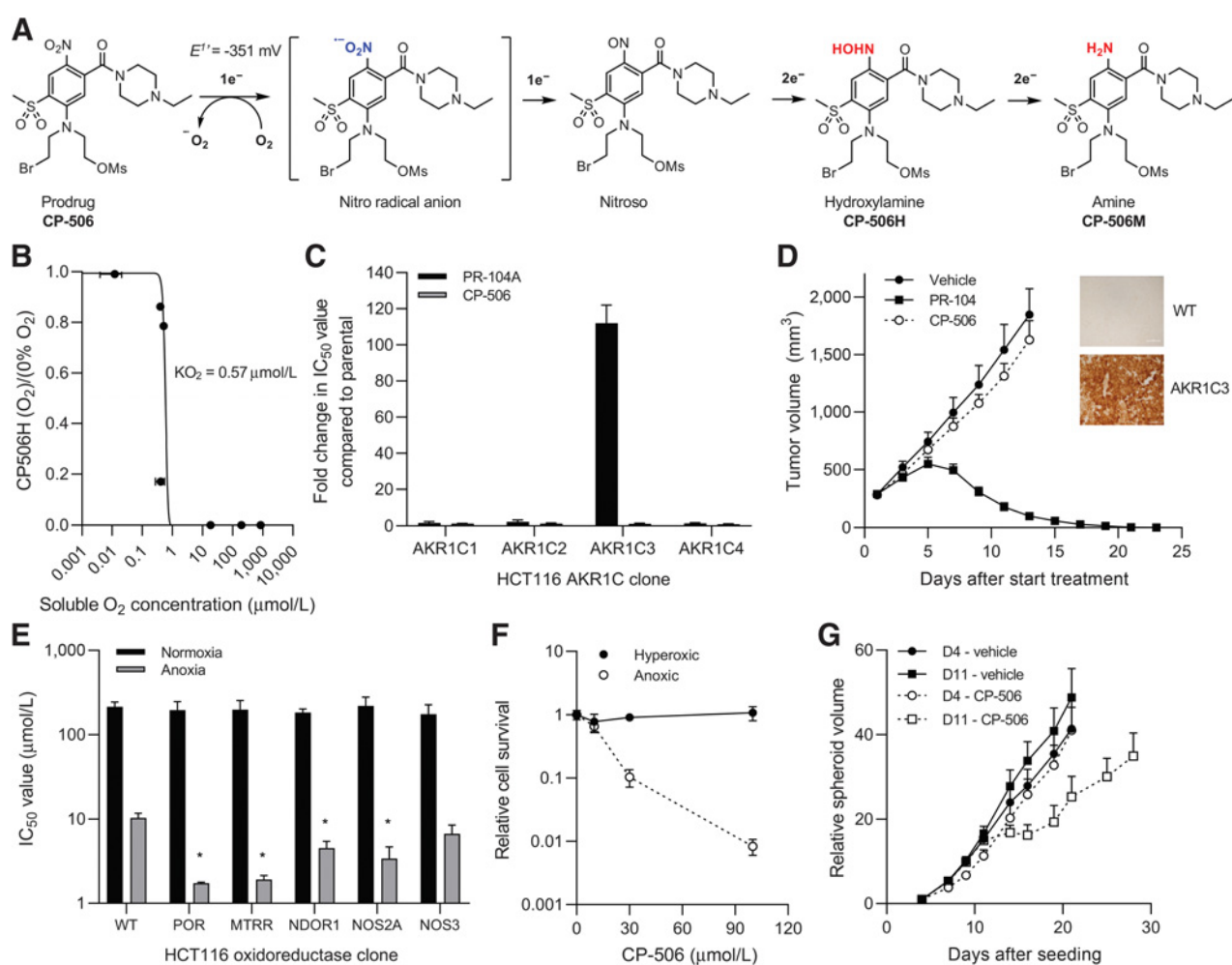


Figure 1. CP-506 is resistant to aerobic activation. **A**, Proposed mechanism of activation of CP-506. **B**, The O_2 -dependence of CP-506 metabolism (CP-506H formation). **C**, Fold-change in IC_{50} values of AKR1C-expressing HCT116 cells exposed to PR-104A or CP-506 compared with parental cells. **D**, Tumor growth of PR-104- and CP-506-treated SNU-398 tumors engineered to express human AKR1C3 as confirmed by IHC detection of AKR1C3 on FFPE tumor sections (image insert; AKR1C3). SNU-398 parental tumors were used as negative control (image insert; WT). **E**, Comparative normoxic and anoxic IC_{50} values of HCT116 cell overexpressing human diflavin oxidoreductases; POR (5.9-fold; $P = 0.008$), MTRR (5.4-fold; $P = 0.008$), NDOR1 (2.3-fold; $P = 0.016$), and NOS2A (3.0-fold; $P = 0.010$), NOS3 ($P = 0.16$). **F**, Clonogenic cell survival of H460 MCLs with differential oxygenation status after 4 hours CP-506 exposure. **G**, Effect of CP-506 on growth of H460 spheroids with differential hypoxic status. Spheroids were treated with CP-506 ($250 \mu\text{mol/L}$) at day 4 (D4; normoxic) or day 11 (D11; hypoxic), after which spheroid growth was monitored. Data are presented as mean \pm SEM.

Spheroid culture

Spheroids were grown as described previously (37). Monitoring of spheroid growth and assessment of oxygenation status is described in Supplementary Materials and Methods. To assess the effect of CP-506 on spheroid growth, normoxic and hypoxic spheroids were treated with CP-506 for 4 hours, after which spheroids received fresh culture medium and growth was monitored.

Animals

All animal experiments were performed with appropriate ethical approval by the University of Auckland Animal Ethics Committee (AEC; approval 001781), the Centrale Commissie Dierproeven (CCD; approval AVD1070020184649), CrownBio CRO AEC (approvals AN-1702-010-113 and AN-1803-13-36), and the Office of Laboratory Animal Welfare [OLAW; approval D16-00682 (A4358-01)] and according to institutional guidelines of The University of Auckland

and the Dier Experimenten Commissie of Maastricht University (DEC-UM; 2013-081, 2014-108, and 2017-030). Additional information on the animal experiments performed in this study are described in Supplementary Table S2.

Pharmacokinetic studies

Pharmacokinetic properties of CP-506 were monitored in NIH-III mice following intravenous, oral, or intraperitoneal administration at indicated time points. Sample collection, LC/MS analysis, and assessment of pharmacokinetic parameters are described in Supplementary Materials and Methods.

Tumor models and treatment schedules

To generate tumors, cells were resuspended in 50% Matrigel (BD Biosciences) or α MEM and injected subcutaneously into the flank of the animal. Mice were randomly assigned to treatment groups upon a

tumor volume of ca. 200 mm³ (treatment starting volume, SV). To evaluate the antitumor effects of CP-506, mice received different dose-regimens of vehicle or CP-506. To investigate the causal relationship between the antitumor effects of CP-506 and tumor oxygenation, mice bearing MDA-468 xenografts were exposed to 7% O₂, 21% O₂, or carbogen (95% O₂, 5% CO₂) and nicotinamide (500 mg/kg, i.p.; Sigma-Aldrich; CarbN) in controlled breathing chambers for a total of 2.5 hours. Thirty minutes after start of modified breathing conditions, vehicle or CP-506 (600 mg/kg, i.p., QD1) were injected. Tumor response was quantified as (i) tumor growth inhibition (TGI) at the day respective control animals reached four times SV (4xSV), (ii) as tumor growth delay (TGD) defined as time to reach 4xSV (T4xSV), or (iii) as specific growth delay (SGD). To estimate and compare the magnitude of treatment effect, the enhancement ratio (ER), defined as the ratio of T4xSV of CP-506-treated animals to T4xSV of vehicle-treated animals, was determined. Assessment of tumor volumes and definition of TGI and SGD are described in Supplementary Materials and Methods.

Tumor excision assay

H460 xenograft-bearing mice were exposed to sham or whole body irradiation (10 Gy), followed by administration of vehicle or CP-506 (900 or 1100 mg/kg, i.p., QD1). 18 hours after, tumors were excised, homogenized, and plated. Clonogenic survival was assessed after 10 days. Log cell kill (LCK) relative to sham-treated controls were calculated.

Assessment of tumor hypoxia and DNA damage

Mice bearing vehicle- or CP-506-treated xenografts were injected with the hypoxia markers pimonidazole (60 mg/kg, i.p. in saline), EF5 (30 mg/kg, i.p. in saline; Sigma-Aldrich) respectively 1 and 3 hours before tumor harvesting, and/or CCI-103F [100 mg/kg, i.p. in 10% (v/v) DMSO in peanut oil; NPI Inc.] 2 hours before the start of treatment depending on the experiment. Subsequent collection and staining of tumors, image acquisition, and analysis are described in Supplementary Materials and Methods.

Statistical analysis

Statistical analyses were performed in GraphPad Prism 8.4.3 software (GraphPad Software, Inc.) or SigmaStat v14.1 (Systat Software). Differences in T4xSV and HF were analyzed using an unpaired *t* test or one-way ANOVA. Differences in survival were analyzed using a log-rank test. *P* values ≤ 0.05 were considered statistically significant. A multivariate linear regression analysis was performed (STATA/IC 11.1) on a dataset comprising data of 381 animals to test which parameters significantly influenced ER or SGD: HF (%), anoxic IC₅₀ (μmol/L), absolute cumulative exposure (mg), and mean volume doubling time (days). Only animals for which all of these variables were available were included in the multivariate linear regression analysis. Furthermore, five additional xenograft models not shown in the main manuscript were included in the model (Supplementary Table S2). Details of this analysis are described in Supplementary Materials and Methods. A nomogram predicting ER was subsequently constructed in R (v4.0.2).

Results

Reduction of CP-506 to its radical anion is inhibited by oxygen

The one-electron reduction potential (E^{θ}) of CP-506 at pH 7 versus normal hydrogen electrode was -351 ± 8 mV (Supplementary Fig. S2A), within the appropriate range to undergo one-electron

reduction by endogenous oxidoreductases. The second-order back-oxidation rate constant of the radical anion by O₂ was determined as $2.45 \pm 0.08 \times 10^6 \text{ M}^{-1} \text{ s}^{-1}$, conformant with other nitroarene prodrugs of similar E^{θ} (Supplementary Fig. S2B). Stepwise reduction of CP-506 upon steady-state radiolysis under anoxia resulted in spectral changes with maintenance of isosbestic points and complete reduction of the compound at $G(\text{loss}) = 1.01 \pm 0.04 \times 10^{-7} \text{ M/Gy}$, requiring six reducing equivalents (Supplementary Figs. S2C and S2D). These data indicate a complete six-electron reduction of the nitro substituent to the amine (CP-506M) and identify it as a probable cytotoxic species formed under anoxic conditions.

Metabolism and cytotoxicity of CP-506 is inhibited by trace oxygen

To evaluate the O₂-dependence of metabolism and cytotoxicity of CP-506, HCT116^{POR} single-cell stirred suspensions were exposed to CP-506 under increasing solution-phase O₂ concentrations. CP-506 concentration declined as function of aqueous soluble O₂ with maximal metabolic consumption achieved under anoxia. Metabolic consumption of CP-506 was accompanied by formation of CP-506H and CP-506M. Data were fitted for CP-506H formation with a four-parameter sigmoidal curve ($R^2 = 0.703$), suggesting a K_{O₂} value of 0.57 μmol/L O₂ with metabolism completely inhibited by soluble O₂ concentrations above 1 μmol/L (Fig. 1B). Consistent with the hypoxia-selective metabolism, the cytotoxicity of CP-506 was maximal in anoxic cultures and was progressively inhibited by increasing solution-phase O₂. The slope of the *k*-curve ($R^2 = 0.504$) suggests a K_{O₂} value of 0.60 μmol/L O₂, with clonogenic killing completely inhibited by O₂ concentrations above 1 μmol/L (Supplementary Fig. S2E). These data indicate that metabolism and cytotoxicity of CP-506 are readily inhibited by trace O₂.

CP-506 is resistant to aerobic activation and is selectively cytotoxic in hypoxic 2D cell cultures

First, to validate that CP-506 is, unlike PR-104A, resistant to aerobic activation by the human two-electron reductase AKR1C3, HCT116 parental (WT) and HCT116 cells overexpressing the AKR1C family members (AKR1C1–AKR1C4) were exposed to each prodrug under normoxic conditions. HCT116^{AKR1C3} cells displayed 112-fold hypersensitivity to PR-104A relative to HCT116^{WT} cells ($P < 0.01$), while the remaining AKR1C-expressing cell lines were refractory (Fig. 1C). In contrast, CP-506 failed to inhibit the proliferation of the AKR1C expressing cells, including HCT116^{AKR1C3} cells. To account for potential differences in metabolite loss, HCT116^{WT} and HCT116^{AKR1C3} 3D MCLs were exposed to 10 μmol/L PR-104A or CP-506 under hyperoxic conditions. Exposure to PR-104A drastically reduced (>99.9%) clonogenic survival of HCT116^{AKR1C3} but not of HCT116^{WT} MCLs, whereas no effect was observed upon CP-506 treatment (Supplementary Fig. S3A). To confirm these findings *in vivo*, isogenic SNU-398 tumors, either AKR1C3-negative parental (WT) or overexpressing AKR1C3 were treated with equimolar doses (950 μmol/kg) of PR-104 or CP-506. SNU-398^{WT} tumors were refractory to either treatment (Supplementary Fig. S3B), whereas SNU-398^{AKR1C3} tumors rapidly regressed upon PR-104, but not CP-506 treatment (Fig. 1D). Similar results were observed in HCT116 isogenic tumor models (Supplementary Fig. S3C and S3D). Taken together, these data confirm that CP-506 is resistant to AKR1C3-mediated aerobic bioactivation.

Next, to determine whether CP-506 is a substrate for endogenous human one-electron oxidoreductases, HCT116 cells overexpressing human diflavin reductases were exposed to CP-506 under normoxia or anoxia. Relative to parental cells, anoxic IC₅₀ values of CP-506 were

significantly ($P \leq 0.01$) lower in HCT116 cells overexpressing POR, MTRR, NDOR1, and NOS2A, but not NOS3, whereas no differences in normoxic IC_{50} values were observed (Fig. 1E). To confirm that CP-506 retains hypoxia-selective cytotoxicity *in vitro*, we assessed normoxic and anoxic IC_{50} values and corresponding HCRs of CP-506 and PR-104A in MDA-468, C33A, and SiHa (Supplementary Figs. S3E–S3G). CP-506 was consistently more cytotoxic under anoxia (HCR: 203, 55, and 20, respectively), whereas PR-104A displayed less hypoxia-selectivity (HCR: 65, 23, and 7, respectively). Lastly, IC_{50} values of CP-506 were determined in a broad panel of human tumor cell lines (Table 1; Supplementary Table S3). For all cell lines, normoxic IC_{50} values were higher than anoxic IC_{50} values, resulting in HCRs ranging from 4 to 157. Complete dose–response curves under normoxic and anoxic conditions of representative cell lines are shown in Supplementary Fig. S4. These data demonstrate the hypoxia-selective bioactivation and cytotoxicity of CP-506 in *in vitro* monolayer cultures.

CP-506-DNA adducts specifically form under hypoxic conditions *in vitro*

To demonstrate hypoxia-selective CP-506-DNA adduct formation, a targeted LC-MS approach focusing on 39 adducts identified earlier was employed. Exposure of cells to CP-506 under normoxic conditions resulted in formation of 2 or 3 DNA monoadducts. In contrast, cells exposed to CP-506 under anoxic conditions demonstrated formation of 9 to 15 DNA adducts, including several crosslinks (Supplementary Table S4). The majority of these adducts were formed due to the activated metabolite CP-506M, followed by CP-506H. Collectively, these data support the hypoxia-specific activation of CP-506 and subsequent DNA adduct formation by its metabolites.

CP-506 is selectively cytotoxic in several hypoxic 3D cell cultures

As the hypoxia-selectivity of CP-506 is reliant on robust tissue penetration properties *in vivo*, we first compared the diffusion of CP-506 and PR-104A across HCT116 3D MCLs under hyperoxic conditions. When compared with PR-104A, CP-506 demonstrated

greater stability in culture medium (Supplementary Fig. S5A) and a 2.2-fold higher diffusion coefficient ($2.75 \pm 0.43 \times 10^{-7}$ vs. $1.26 \pm 0.14 \times 10^{-7}$ cm^2/s ; Supplementary Fig. S5B and S5C). CP-506 thus exhibits excellent transport properties, a requirement for improved HAP performance. The superior aqueous stability of CP-506 also extended to human and mouse plasma stability, with no detectable loss of CP-506 (Supplementary Fig. S5D).

In line with data obtained in 2D cell cultures, we demonstrated that CP-506 had no cytotoxic effects in hyperoxic H460 MCLs. In anoxic MCLs, however, a concentration-dependent decrease in clonogenic cell survival was observed (Fig. 1F). In addition, H460 spheroids were exposed to CP-506, as spheroids naturally develop a diffusion-limited hypoxic core as they grow (Supplementary Fig. S5E). Growth inhibition was observed in hypoxic (day 11), but not normoxic (day 4) spheroids upon treatment with CP-506 (Fig. 1G). Overall, these data confirm the hypoxia-selectivity of CP-506 using 3D *in vitro* cell culture models.

Pharmacokinetic analysis of CP-506

Modeling of plasma concentrations of CP-506 following intravenously and orally dosing (383 mg/kg; Supplementary Fig. S6A) demonstrated oral bioavailability (F_{abs}) of 47% with a half-life ($T_{1/2}$) of 0.92 hours (Supplementary Table S5). Next, the plasma concentration–time profile of CP-506 was assessed using intraperitoneally dosing (600 or 800 mg/kg; 50% and 67% of MTD, respectively), demonstrating maximum plasma concentrations (C_{max}) of 246.2 $\mu mol/L$ (600 mg/kg) and 353.8 $\mu mol/L$ (800 mg/kg) with a calculated $T_{1/2}$ of 0.54 to 0.58 hours. The area under the plasma concentration–time extrapolated to infinity (AUC_{0-inf}) was 206.7 $\mu mol.h/L$ (600 mg/kg) and 276.3 $\mu mol.h/L$ (800 mg/kg; Supplementary Fig. S6B).

The antitumor effects of CP-506 are causally related to tumor oxygenation

To investigate the capacity of HAP to preferentially sterilize hypoxic, radiation-resistant tumor cells, we first assessed the spatial relationship between tumor hypoxia and DNA damage in DMS114

Table 1. IC_{50} values in normoxic (21% O_2) and anoxic ($\leq 0.02\%$ O_2) *in vitro* monolayers after 4 hours exposure to CP-506.

Cell line	Cancer type	NIC_{50} ($\mu mol/L$)	AIC_{50} ($\mu mol/L$)	HCR
SW1990	Pancreatic adenocarcinoma	133	1.7	78.8
DMS 114	Small cell lung carcinoma	360	3.6	100
MiaPaCa-2	Pancreatic ductal adenocarcinoma	646	4.1	157
MDA-468	Breast adenocarcinoma	243	4.7	51.6
H69	Small cell lung carcinoma	59	7.3	8.1
MDA-436	Breast adenocarcinoma	178	17.5	10.2
H460	Large cell lung carcinoma	319	18.4	17.4
SiHa	Cervix squamous cell carcinoma	459	22.5	20.4
BT-474	Breast ductal adenocarcinoma	1500	27.0	55.5
H1650	Lung adenocarcinoma	835	40.0	20.9
A2780*	Ovarian carcinoma	244	49.0	5.0
Panc-1	Pancreatic ductal adenocarcinoma	464	59.1	7.9
HCT116*	Colorectal carcinoma	>500	64.0	7.8
MDA-231	Breast adenocarcinoma	663	92.9	7.1
FaDu*	Head and neck squamous cell carcinoma	>500	196.0	2.6

Note: Cell viability was assessed 96 hours after the start of treatment using the CellTiter-Glo assay. Normoxic (NIC_{50}) and anoxic (AIC_{50}) IC_{50} values were subsequently determined on the basis of independent biological replicates ($n \leq 3$). The hypoxia cytotoxicity ratio (HCR) was obtained by dividing the normoxic IC_{50} by the corresponding anoxic IC_{50} . An asterisk (*) indicates the cell viability assay was performed using the alamarBlue reagent. A complete summary of IC_{50} values of all cell lines tested ($n = 51$) can be found in Supplementary Table S3.

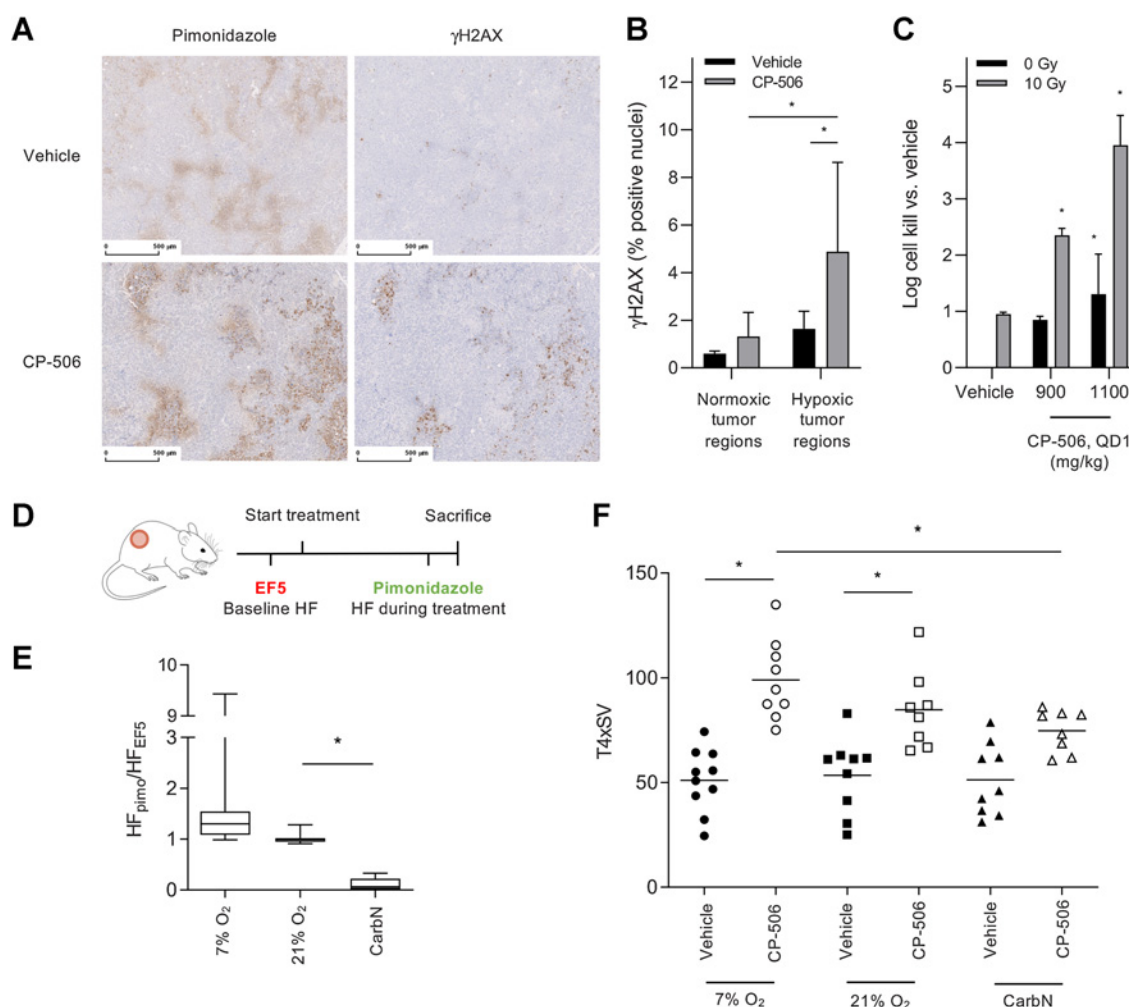


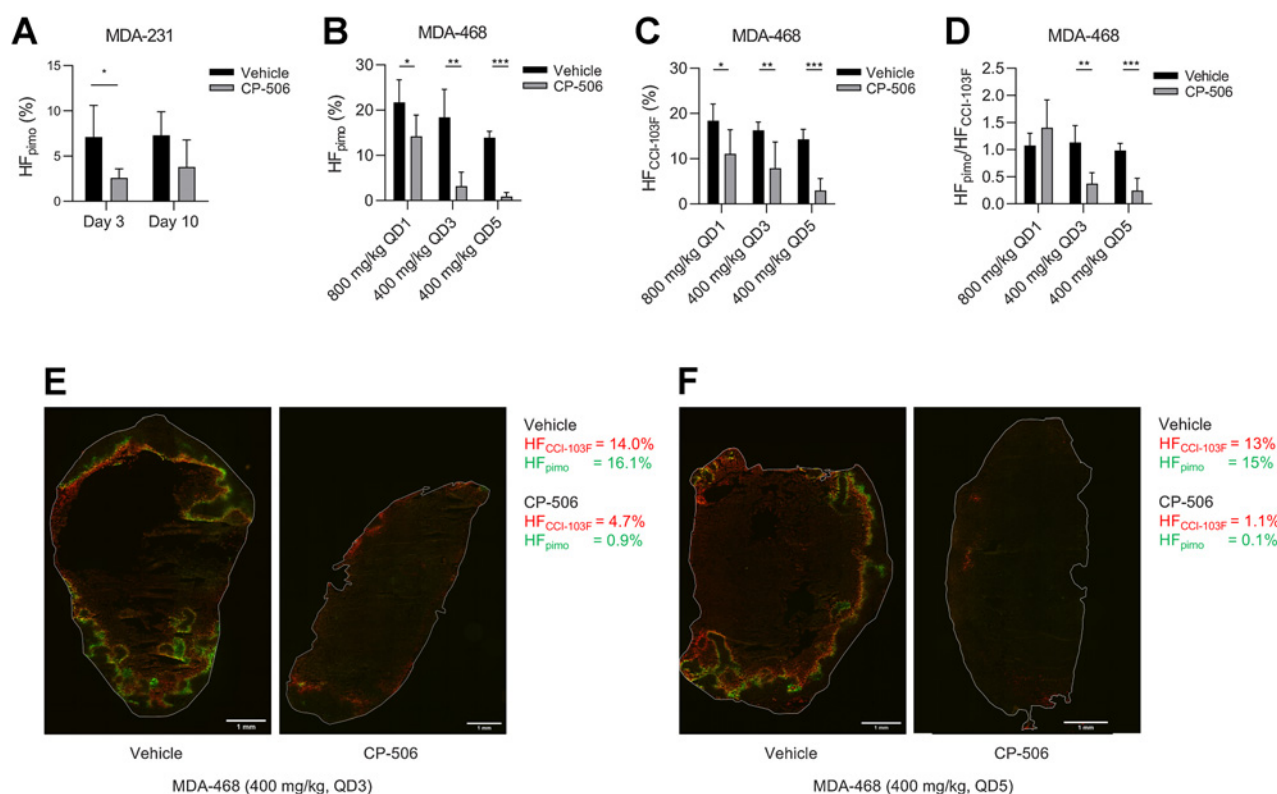
Figure 2.

The antitumor effects of CP-506 are causally related to tumor oxygenation. **A**, DMS114 tumors were exposed to vehicle or CP-506 (600 mg/kg, QD1), after which tumor hypoxia (pimonidazole) and DNA damage (γ H2AX) were assessed and (**B**) quantified. **C**, Excision assay of H460 tumors treated with radiation (10 Gy) and/or single dose CP-506 (900 or 1100 mg/kg, i.p.). **D**, Animals bearing MDA-468 tumor xenografts were exposed to modified breathing strategies [i.e., 7% O₂, 21% O₂, and carbogen (95% O₂, 5% CO₂) and nicotinamide (500 mg/kg) (CarbN)], during which CP-506 (600 mg/kg) was administered. **E**, Ratios of HF_{pimo}/HF_{EF5} of vehicle-treated tumors. The boxplot represents Q1, median, and Q3. Bars indicate the minimum and maximum values ($n = 6$ animals per treatment condition). **F**, Tumor growth was assessed and time to reach four times starting volume (T4xSV) was calculated. Data are presented as mean \pm SD.

xenograft-bearing mice exposed to CP-506 (600 mg/kg, QD1, IP). CP-506 specifically induced DNA damage (γ H2AX) in hypoxic (pimonidazole-positive) regions (Fig. 2A and B). Second, we exposed H460 xenograft-bearing mice to single-dose (10 Gy) irradiation (IR) followed by administration of CP-506 (900 or 1100 mg/kg, QD1, IP). IR provided 0.95 LCK, which was amplified to 2.36 and 3.95 LCK ($P < 0.01$), respectively, by subsequent administration of CP-506 (Fig. 2C). Administration of CP-506 alone resulted in 0.84 and 1.30 LCK, respectively. CP-506 thus demonstrated greater cell killing within the hypoxic, radiation-resistant tumor subpopulation than across the whole tumor cell population. Taken together, these data indicate that CP-506 preferentially exerts its antitumor effects in the hypoxic regions of the tumor.

The causal relationship between tumor oxygenation and antitumor effects of CP-506 was assessed in MDA-468 xenograft-bearing mice exposed to 7% O₂, 21% O₂, or CarbN breathing conditions during

which CP-506 (600 mg/kg, QD1, IP) was administered. Besides tumor growth monitoring, changes in HF were assessed in sentinel animals injected with the hypoxia markers EF5 1 hour before the start of modified breathing conditions (HF_{EF5}) and pimonidazole 1 hour before euthanasia, immediately after treatment (HF_{pimo}; Fig. 2D). In vehicle-treated mice, no difference was observed between HF_{pimo} and HF_{EF5} (median HF_{pimo}/HF_{EF5} = 1.0; IQR = 0.07) in animals exposed to 21% O₂ breathing conditions. Exposure to 7% O₂ increased HF_{pimo}/HF_{EF5} (median = 1.25; IQR = 0.46) albeit not significantly ($P = 0.16$), whereas CarbN exposure significantly decreased HF_{pimo}/HF_{EF5} (median = 0.06, IQR = 0.2; $P < 0.0001$; Fig. 2E; Supplementary Fig. S7A). HF_{pimo}/HF_{EF5} ratios of CP-506-treated mice are presented in Supplementary Fig. S7B. Administration of CP-506 increased T4xSV to a higher extent in animals exposed to 7% (100.1 \pm 19.1 vs. 51.4 \pm 14.8 days, $P < 0.0001$) compared with animals exposed to 21% O₂ (87.5 \pm 15.7 vs. 54.0 \pm 15.0 days, $P < 0.01$) and CarbN (76.3 \pm

**Figure 3.**

Impact of CP-506 on the hypoxic fraction in *in vivo* tumor xenografts. **A**, Hypoxic fraction as assessed by pimonidazole positivity in MDA-231 tumor xenografts 3 and 10 days after the end of CP-506 treatment (800 mg/kg, QD5). HF of MDA-468 tumors as assessed by **(B)** pimonidazole (HF_{pimo}) and **(C)** CCI-103F (HF_{CCI-103F}) positivity at the end of different treatment schedules. **D**, The ratio of HF_{pimo} to HF_{CCI-103F} of MDA-468 tumors after different treatment schedules. **E**, Representative images of tumor hypoxia assessed by pimonidazole (green) and CCI-103F (red) positivity in MDA-468 tumors (delineated in white) treated with vehicle or CP-506 (400 mg/kg, QD3) and **(F)** vehicle or CP-506 (400 mg/kg, QD5). Data are presented as mean \pm SD.

9.0 vs. 53.8 ± 19.1 days, $P = 0.0781$; **Fig. 2F**). These data demonstrate a causal relationship between the antitumor effects of CP-506 and tumor oxygenation status.

CP-506 eradicates hypoxic tumor cells in a dose-dependent manner

To further investigate the hypoxia-selective antitumor effects of CP-506, we first characterized the effects of CP-506 (800 mg/kg, QD5, IP) on the HF of MDA-231 xenografts. CP-506 decreased HF from $7.1 \pm 3.5\%$ to $2.6 \pm 1.5\%$ ($P < 0.05$) 3 days post-treatment, and from $7.3 \pm 2.6\%$ to $3.8 \pm 3.1\%$ ($P = 0.21$) 10 days post-treatment, indicating a time-dependent CP-506-mediated decrease in HF (**Fig. 3A**). Next, changes in HF in MDA-468 tumor xenografts were evaluated using a double hypoxia marker approach to investigate whether pimonidazole-positive cells were already present (pimonidazole- and CCI-103F-positive) at start of treatment, or if they were formed posttreatment (pimonidazole positive and CCI-103-negative). Different dosing regimens were tested (800 mg/kg, QD1; 400 mg/kg, QD3; 400 mg/kg, QD5; all IP). CP-506 significantly decreased HF_{CCI-103F} and HF_{pimo} (**Fig. 3B and C**), and the ratio of HF_{pimo} to HF_{CCI-103F} (**Fig. 3D**), all in a dose-dependent manner, suggesting effective eradication of hypoxic tumor cells. Representative images are shown in **Fig. 3E and F**. Taken together, these data indicate that CP-506 eradicates hypoxic tumor cells.

CP-506 exhibits dose-dependent and broad single-agent antitumor activity

To characterize the single-agent activity of CP-506 and determine the optimal dose regimen, we first treated H69 small-cell lung cancer xenografts with various schedules of CP-506 (600 mg/kg, IP; **Fig. 4** and Supplementary Table S5). An increased number of consecutive administrations was associated with increased depth of response (**Fig. 4A**). This was also reflected in T4xSV, where QD5 resulted in a higher T4xSV (30.2 ± 6.9) compared with QD3 (22.9 ± 5.5 ; **Fig. 4B**). Furthermore, consecutive dose-scheduling (QD5) provided superior tumor control compared with intermittent dose-scheduling (QW5; T4xSV = 22.0 ± 8.1 ; **Fig. 4A and B**). Repeated consecutive dose-schedules provided extended tumor control and further increased T4xSV (QD5 \times 3: 52.6 ± 15 ; QD3 \times 5: 44.8 ± 5.6 ; **Fig. 4A and B**). Comparable results were observed for ER (Supplementary Table S6). Importantly, daily dosing was well-tolerated with transient body weight loss (Supplementary Fig. S8A). A dose regimen of a single CP-506 dose for five consecutive days (QD5) was selected for subsequent experiments. Next, we investigated whether CP-506 exhibited dose-dependent antitumor effects. MDA-468 xenograft-bearing mice were treated with increasing doses of CP-506 (200–800 mg/kg, QD5, i.p.). CP-506 exhibited dose-dependent TGD (T2xSV; **Fig. 5A**) and TGI at day 47 (final common monitoring time of all treatment arms) of 12.3% (200 mg/kg), 58.5% (400 mg/kg), 88.9% (600 mg/kg), and 99.7%

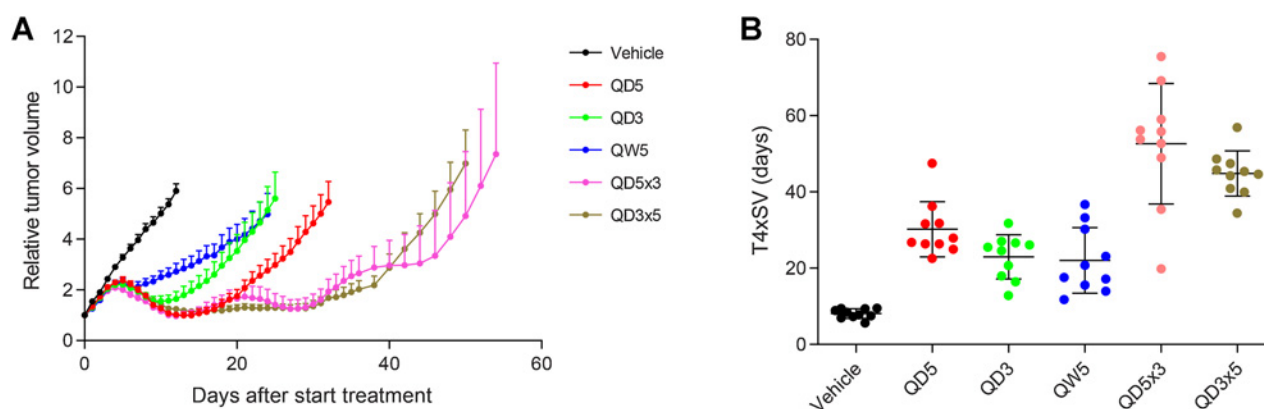


Figure 4.

The antitumor effects of different dose regimens of CP-506. Mice bearing H69 tumor xenografts were treated with different dose regimens of CP-506 (600 mg/kg, i.p.), after which (A) tumor growth was assessed. B, Individual tumor responses are shown as T4xSV (time to reach 4× start volume). Schedules were QD5: a single injection per day for 5 consecutive days; QD3: a single injection per day for 3 consecutive days; QW5: a single injection per week for 5 consecutive weeks; QD5×3: a single injection per day for 5 consecutive days per week, repeated 3 weeks; QD3×5: a single injection per day for 3 consecutive days per week, repeated 5 weeks. Data are presented as mean ± SEM ($n = 10$ animals per treatment condition).

(800 mg/kg). Vehicle-treated animals and animals treated with 600 or 800 mg/kg were monitored for a prolonged time period. Administration of 600 mg/kg CP-506 increased T4xSV significantly (163.2 ± 33.3 days) compared with vehicle-treated tumors (94.0 ± 11.4 days; $P < 0.0001$). Administration of 800 mg/kg resulted in complete and maintained long-term responses in 9 of 10 animals (Fig. 5A; Supplementary Fig. S8B).

Finally, to broadly characterize the single-agent antitumor activity of CP-506 *in vivo*, animals bearing a wide range of human tumor xenografts were treated with CP-506 (600 or 800 mg/kg, QD5, IP). The tumor models were selected on the basis of their *in vitro* sensitivity to CP-506 and were characterized by varying degrees of tumor hypoxia (Fig. 5B). In all models, CP-506 was well-tolerated with transient body weight loss during the treatment period. CP-506 effectively inhibited tumor growth in 13 of 15 models tested, with TGIs ranging from 30.9% to 99.3% (Fig. 5C; Supplementary Table S6), and significantly increased T4xSV in 12 out of 15 models tested, with calculated ERs ($T4xSV_{CP-506}/T4xSV_{vehicle}$) ranging from 1.3 to 3.3 (Supplementary Fig. S9; Supplementary Table S7). In line with previous data, administration of CP-506 resulted in complete regression of 9 of 10 animals bearing MDA-468 xenografts. T4xSV of BT-474 xenografts could not be determined due to short follow-up. Consistently, the only tumor models in which a complete lack of response was observed, MIA PaCa-2 and SW1990, demonstrated no detectable pimonidazole-positive hypoxia or expression of the endogenous hypoxia marker CAIX at the start of treatment (Supplementary Fig. S10), supporting the interpretation that the presence of hypoxia is an absolute requirement for CP-506 to exert its antitumor effects *in vivo*.

Baseline tumor hypoxia and *in vitro* sensitivity are correlated with the treatment response to CP-506

To identify which factors contribute to the tumoral response to CP-506, defined as ER or SGD, a multivariate linear regression analysis was performed. ER was positively correlated with baseline HF ($P < 0.0005$) and negatively correlated with the *in vitro* sensitivity (anoxic IC_{50} ; $P < 0.0005$). A higher CP-506 dose was associated with a higher ER ($P < 0.0001$). Similar results were obtained using SGD as outcome variable. Using these significantly variables, a nomogram was constructed allowing ER prediction (Supplementary Fig. S11). Taken

together, these data demonstrate that the degree of tumor hypoxia and the *in vitro* sensitivity to CP-506 are significantly correlated to the treatment response.

Discussion

In this study, we evaluated the therapeutic potential of the hypoxia-activated DNA crosslinking prodrug CP-506, designed to lack off-mechanism aerobic metabolism unlike its predecessor PR-104 (23), whereas concurrently possessing superior physicochemical and pharmacokinetic properties, including improved solubility, stability, tissue diffusion, and oral bioavailability.

CP-506 exhibited a one-electron affinity (E^{θ}) optimal for reduction by human endogenous single-electron oxidoreductases, and a back-oxidation rate constant that indicates efficient competition with molecular oxygen. Further, direct measurements of metabolism and cytotoxicity of CP-506 using stirred cell suspensions with accurate, real-time measurements of soluble O_2 concentrations confirmed the strict hypoxia-dependent bioactivation of CP-506, which was completely inhibited at O_2 concentrations above $1 \mu\text{mol/L}$ (0.1% O_2). CP-506 demonstrates an unusually steep k -curve providing optimal selectivity for pathological hypoxia. Consequently, although its KO_2 value is only two-fold lower than that of tirapazamine (38), CP-506 is fully and completely inhibited at O_2 concentrations 100-fold lower ($1 \mu\text{mol/L}$ vs. $100 \mu\text{mol/L}$ O_2 , respectively; Supplementary Fig. S12).

In a wide variety of *in vitro* 2D monolayer cell cultures of different origin, we showed that CP-506 exerts its cytotoxic effects selectively under anoxic conditions, with HCRs ranging from 4 to 203. These results are in line with HCRs previously reported and confirmed here in side-by-side analysis for PR-104A, ranging from 6 to 160 (18), but lower when compared the HAP evofosfamide, with reported HCRs up to 600 (39). This finding may be explained by differences in the bystander effects of CP-506 and evofosfamide: the bystander effect of CP-506 allows escape and dilution of its metabolites into surrounding medium, whereas the activated metabolite of evofosfamide remains largely entrapped in the cell of origin (17), exerting maximal cytotoxicity at the source of metabolism and giving rise to amplified HCRs. The discordant influence of the bystander effect on these 2D

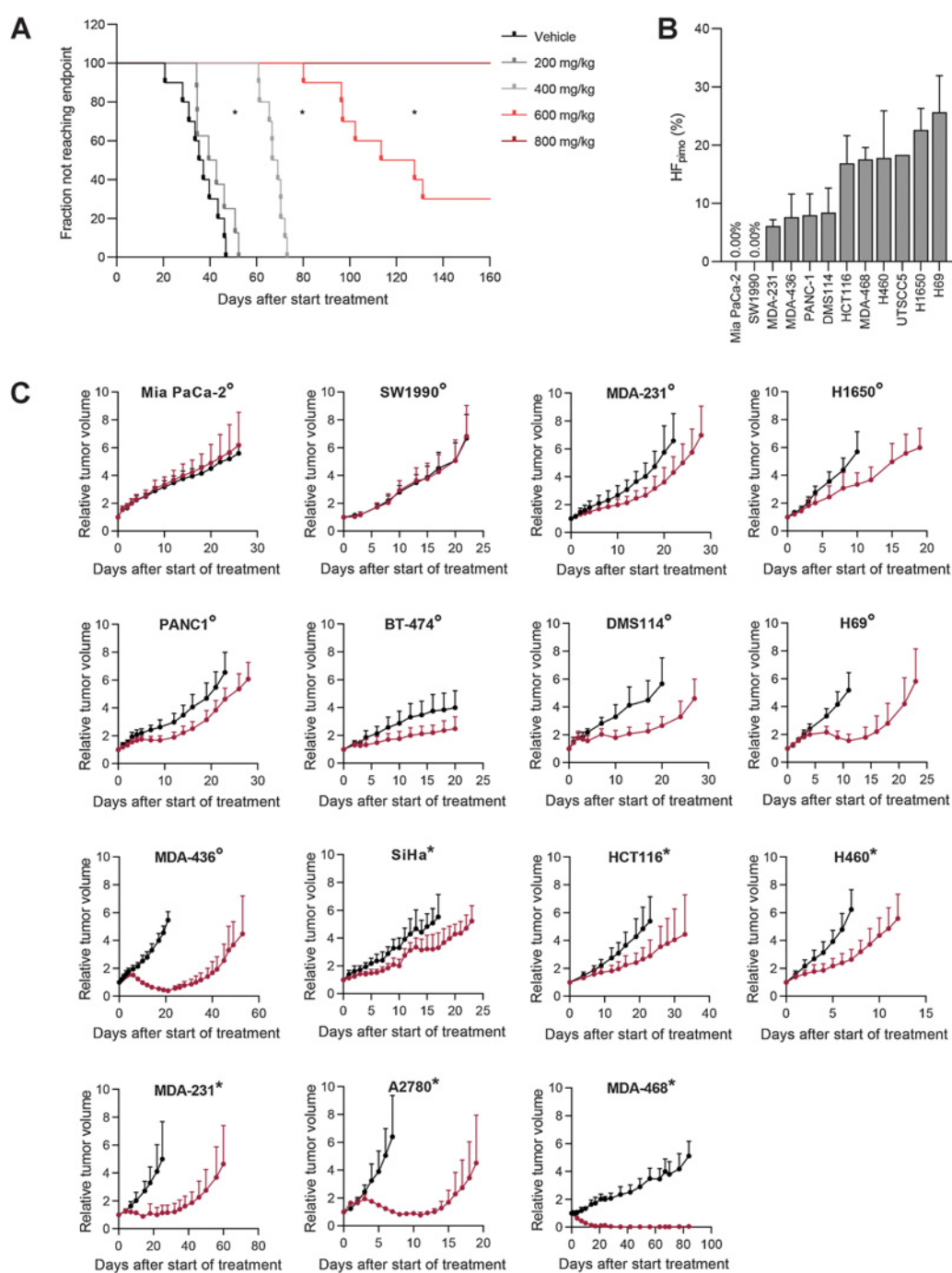


Figure 5. CP-506 inhibits tumor growth of several human xenografts. **A**, Dose-dependence of the antitumor effect of CP-506 in MDA-468 tumor xenografts. Animals bearing MDA-468 xenografts were treated with increasing doses of CP-506 (200–800 mg/kg, i.p., QD5). Tumor growth was assessed and Kaplan–Meier survival plots were constructed. Endpoint is defined as two times starting volume (SV). **B**, HF as assessed by pimonidazole (pimo) positivity of 12 tumor xenograft models. **C**, CP-506 [600 (°) or 800 (°) mg/kg, i.p.] was administered once per day for 5 days (QD5) in 15 different xenograft models. Tumor growth was monitored and TGD, defined as the time to reach four times start volume (T4xSV), was determined. Data are presented as mean ± SD.

assays therefore limits accurate comparison of the hypoxia-selectivity of HAPs with diverse physicochemical properties. To address this experimental limitation, we confirmed the hypoxia-selectivity of CP-506 in several 3D *in vitro* cell culture models,

which mimic the structure of the *in vivo* tumor environment more closely than 2D monolayers (40).

In vivo, CP-506 demonstrated potent single-agent antitumor activity at well-tolerated doses in 13 hypoxic xenograft models tested. In

line with this, HAPs such as PR-104 (18) and evofosfamide (7) have also displayed strong monotherapeutic antitumor effects. However, it is understood that the antitumor effects of PR-104 and evofosfamide are not solely due to their HAP behavior: PR-104 single-agent activity is dominated by the unforeseen oxygen-independent metabolism by AKR1C3 (23), whereas the single-agent activity of evofosfamide is mediated by background activation in normoxic tumor regions likely due to inadequate inhibition by O₂ (17). Importantly, we establish here that CP-506 is resistant to AKR1C3 reductive metabolism and is fully quenched by 1 μmol/L O₂. PR-104 is not a substrate for the murine orthologues, resulting in favorable murine toxicokinetics (26) that failed to translate to human dose tolerance in phase I trials (21, 22). Thus, without the confounding factor of human aerobic AKR1C3 metabolism, it is reasonable to anticipate that the interspecies allometric scaling of CP-506 will extrapolate in a predictable manner (41).

Several factors have been proposed to influence the *in vivo* antitumor effects of HAPs (42), including the extent of tumor hypoxia. Indeed, in a monotherapy study employing eight different xenograft models, Sun and colleagues found a good correlation between baseline tumor hypoxia and evofosfamide (7), confirmed later in a different study employing modified breathing strategies (9). Here, by using similar modified breathing strategies, we demonstrated that the efficacy of CP-506 increased as function of HF in MDA-468 tumor xenografts. Moreover, in a multivariate linear regression analysis employing data of 15 different tumor models, we showed that pretreatment tumor hypoxia as well as intrinsic cellular sensitivity to CP-506 strongly correlated with tumor response. Consistently, our results also indicate that hypoxia is an absolute prerequisite for CP-506 to exert its antitumor effects as the MIA PaCa-2 and SW1990 pancreatic tumor models, despite their significant cellular sensitivity to CP-506 *in vitro* (Table 1), exhibited a complete lack of response *in vivo* associated with total absence of hypoxia. Further supportive of the hypoxia-mediated mechanism of action of CP-506 is the spatial relationship of tumor hypoxia and accumulated DNA damage, a greater cell kill observed within the radiation resistant, hypoxic tumor subpopulation, and a dose-dependent decrease in tumor HF.

Because HAPs require an initial activation step by endogenous one-electron oxidoreductases, the levels and catalytic activity of prodrug-activating nitroreductases are a second factor likely contributing to HAP efficacy (35, 43, 44). Here, we identified cytochrome P450 oxidoreductase (POR), methionine synthase reductase (MTRR), novel diflavin oxidoreductase 1 (NDOR1), and inducible nitric oxide synthase (NOS2A) as likely candidates, although it should be noted that one-electron oxidoreductases responsible for HAP activation can exhibit functional redundancy (42). In addition, the intrinsic sensitivity to the activated, cytotoxic metabolites of CP-506 is likely to influence its antitumor effects. For PR-104 and evofosfamide, it has been shown that tumors deficient in homologous recombination (HR) are markedly more sensitive to HAP treatment (20, 39, 45). As CP-506 is a hypoxia-activated DNA alkylating agent that exerts its cytotoxicity by the formation of DNA interstrand crosslinks and subsequent induction of DNA double-strand breaks following replication fork stalling, the integrity of DNA repair mechanisms such as the above-mentioned HR and the Fanconi anemia (FA) pathway is likely an important factor in determining the efficacy of CP-506 (46). Of interest and in line with this, we recently discovered (not included in this study) that the MDA-468 cell line is defective in the FA pathway (truncated FANCA gene = Q869*) likely explaining its sensitivity *in vitro* and— together with its high hypoxic fraction—*in vivo*. Experiments to investigate the influence of oxidoreductase expression and activity,

and integrity of the DNA repair response on the sensitivity to CP-506 are currently ongoing.

To date, HAP clinical trials have yielded disappointing results, with a lack of patient stratification accountable for their failure (3). Therefore, gaining a greater mechanistic understanding of the factors and their complex interplay in determining the antitumor effects of CP-506 is essential for successful clinical translation. Despite the clear monotherapeutic activity of CP-506, it should be noted that the therapeutic efficacy of HAPs is predicted to be the greatest when combined with other treatment modalities such as chemo- and radiotherapy (47). Because HAPs mainly target the hypoxic tumor cells, the therapeutic potential can theoretically be enhanced by a different treatment modality that kills aerobic cells. Currently, experiments assessing the effects of the combination of CP-506, radiotherapy, and/or immunotherapy are ongoing.

In conclusion, CP-506 is a novel HAP specifically designed to have a strict *k*-curve that is offset by a bystander effect (36), with aqueous solubility, oral bioavailability, and, importantly, no off-mechanism activation by the human aerobic reductase AKR1C3. Here, we demonstrated that CP-506 selectively kills hypoxic tumor cells and inhibits growth and clonogenic survival of hypoxic spheroids only. *In vivo*, CP-506 demonstrated potent antitumor effects in a broad range of tumor xenograft models. A causal relationship was established between tumor oxygenation and antitumor effects of CP-506 in MDA-468 xenografts as well as significant correlation between baseline hypoxia and tumor response across different tumor types using a multivariate approach. Several other factors besides tumor hypoxia are proposed to influence the tumor response to CP-506. In this light, a strong mechanistic understanding will facilitate the development of predictive or prognostic biomarkers of response critical for successful clinical translation. It is anticipated that the upcoming clinical evaluation of CP-506 will utilize these newly discovered biomarkers of CP-506 response to guide future patient selection.

Authors' Disclosures

A.M. Mowday reports grants from Health Research Council of New Zealand (17/225), Convert Pharmaceuticals, and Health Innovation Ventures during the conduct of the study; also has a patent for EP2888227B1 issued and licensed to Health Innovation Ventures, a patent for US10202408B2 issued and licensed to Health Innovation Ventures, a patent for CA2886574C issued and licensed to Health Innovation Ventures, a patent for US9873710B2 issued and licensed to Health Innovation Ventures, a patent for AU2013/306514B2 issued and licensed to Health Innovation Ventures, and a patent for US9505791B2 issued and licensed to Health Innovation Ventures. X. Lin reports grants from The Health Research Council of New Zealand (17/225), Convert Pharmaceuticals, and Health Innovation Ventures during the conduct of the study. S. Kumara reports grants from Cancer Society of New Zealand during the conduct of the study. A. Ashoorzadeh reports grants from The Health Research Council of New Zealand (17/225), Convert Pharmaceuticals grant, and Health Innovation Ventures grant during the conduct of the study; also has a patent for EP2888227B1 issued and licensed to Health Innovation Ventures, a patent for US10202408B2 issued and licensed to Health Innovation Ventures, a patent for CA2886574C issued and licensed to Health Innovation Ventures, a patent for US9873710B2 issued and licensed to Health Innovation Ventures, a patent for AU2013/306514B2 issued and licensed to Health Innovation Ventures, and a patent for US9505791B2 issued and licensed to Health Innovation Ventures. K.O. Hicks reports grants from The Health Research Council of New Zealand (17/225), Convert Pharmaceuticals grant, and Health Innovation Ventures grant during the conduct of the study. M.R. Bull reports grants from The Health Research Council of New Zealand (17/225), Convert Pharmaceuticals, and Health Innovation Ventures during the conduct of the study. C.P. Guise reports grants from The Health Research Council of New Zealand (17/225), Convert Pharmaceuticals, and Health Innovation Ventures during the conduct of the study; in addition, C.P. Guise has a patent for EP2888227B1 issued and licensed to Health Innovation Ventures, a patent for US10202408B2 issued and licensed to Health Innovation Ventures, a patent for CA2886574C issued and licensed to Health Innovation Ventures, a patent for US9873710B2 issued and licensed

to Health Innovation Ventures, a patent for AU2013/306514B2 issued and licensed to Health Innovation Ventures, and a patent for US9505791B2 issued and licensed to Health Innovation Ventures. S. Deschoemaeker reports grants from Walloon Region of Belgium and personal fees from Convert Pharmaceuticals during the conduct of the study; also has a patent for WO2019229195A1 pending. M.J. Solivio reports personal fees from Convert Pharmaceuticals during the conduct of the study. J.B. Small reports grants from The Health Research Council of New Zealand, Convert Pharmaceuticals, and Health Innovation Ventures during the conduct of the study; personal fees from Convert Pharmaceuticals, Rain Therapeutics, and Kezar Life Sciences; and nonfinancial support from Rain Therapeutics outside the submitted work; also has a patent for EP2888227B1 issued and licensed to Health Innovation Ventures, a patent for US10202408B2 issued and licensed to Health Innovation Ventures, a patent for CA2886574C issued and licensed to Health Innovation Ventures, a patent for US9873710B2 issued and licensed to Health Innovation Ventures, a patent for AU2013/306514B2 issued and licensed to Health Innovation Ventures, and a patent for US9505791B2 issued and licensed to Health Innovation Ventures. J. Theys and L.J. Dubois report other support from Convert Pharmaceuticals during the conduct of the study. A.V. Patterson reports grants from Health Research Council of New Zealand and Health Innovation Ventures, grants and personal fees from Convert Pharmaceuticals during the conduct of the study; grants, personal fees, and nonfinancial support from Rain Therapeutics outside the submitted work; also has a patent for EP2888227B1 issued and licensed to Health Innovation Ventures, a patent for US10202408B2 issued and licensed to Health Innovation Ventures, a patent for CA2886574C issued and licensed to Health Innovation Ventures, a patent for US9873710B2 issued and licensed to Health Innovation Ventures, a patent for AU2013/306514B2 issued and licensed to Health Innovation Ventures, and a patent for US9505791B2 issued and licensed to Health Innovation Ventures. P. Lambin reports other support from Convert Pharmaceuticals during the conduct of the study. No disclosures were reported by the other authors.

Authors' Contributions

A.M.A. van der Wiel: Data curation, formal analysis, investigation, visualization, methodology, writing—original draft, writing—review and editing. **V. Jackson-Patel:** Data curation, software, formal analysis, supervision, validation, investigation, visualization, methodology, writing—original draft, writing—review and editing. **R. Niemans:** Data curation, formal analysis, investigation, visualization, methodology, writing—review and editing. **A. Yaromina:** Conceptualization, data curation, software, formal analysis, supervision, validation, investigation, visualization, methodology, writing—original draft, writing—review and editing. **E. Liu:** Data curation, software, formal analysis, investigation, methodology, writing—original draft. **D. Marcus:** Data curation, investigation, methodology. **A.M. Mowday:** Resources, data curation, formal analysis, validation, investigation, visualization, methodology. **N.G. Lieuwes:** Data curation, investigation, methodology. **R. Biemans:** Data curation, software, formal analysis, validation, investigation, visualization, methodology. **X. Lin:** Data curation, investigation, visualization, methodology. **Z. Fu:** Resources, investigation, visualization, methodology. **S. Kumara:** Data curation, formal analysis, investigation, methodology. **A. Jochems:** Data curation, formal analysis, investigation, methodology. **A. Ashoorzadeh:** Data curation, formal anal-

ysis, validation, investigation, methodology, writing—original draft. **R.F. Anderson:** Data curation, software, formal analysis, investigation, methodology, writing—original draft. **K.O. Hicks:** Conceptualization, software, supervision, validation, methodology, writing—original draft. **M.R. Bull:** Data curation, software, formal analysis, investigation, visualization, methodology, writing—original draft. **M.R. Abbattista:** Data curation, formal analysis, validation, investigation, visualization, methodology. **C.P. Guise:** Data curation, formal analysis, supervision, validation, investigation, visualization, methodology, writing—original draft. **S. Deschoemaeker:** Data curation, formal analysis, investigation, methodology, writing—original draft. **S. Thiolloy:** Data curation, formal analysis, supervision, investigation, visualization, methodology, writing—original draft, project administration. **A. Heyerick:** Conceptualization, resources, data curation, formal analysis, supervision, funding acquisition, validation, investigation, methodology, writing—original draft, project administration. **M.J. Solivio:** Data curation, formal analysis, investigation, visualization, methodology, writing—original draft. **S. Balbo:** Data curation, formal analysis, investigation, visualization, methodology, writing—original draft. **J.B. Small:** Conceptualization, resources, data curation, formal analysis, supervision, funding acquisition, validation, visualization, methodology, writing—original draft, project administration, writing—review and editing. **J. Theys:** Data curation, formal analysis, supervision, investigation, visualization, methodology, writing—review and editing. **L.J. Dubois:** Conceptualization, data curation, formal analysis, supervision, validation, investigation, visualization, methodology, writing—original draft, project administration, writing—review and editing. **A.V. Patterson:** Conceptualization, resources, data curation, formal analysis, supervision, funding acquisition, validation, investigation, visualization, methodology, writing—original draft, project administration, writing—review and editing. **P. Lambin:** Conceptualization, resources, data curation, formal analysis, supervision, funding acquisition, validation, investigation, visualization, methodology, writing—original draft, project administration, writing—review and editing.

Acknowledgments

Prof. M. Losen and Ms. H. Steinbusch from the Department of Psychiatry and Neuropsychology, School for Mental Health and Neuroscience, Maastricht University, are greatly acknowledged for their technical support with microscope image acquisition. This work was supported by the Health Research Council of New Zealand (Grant No. 17/255), ERC advanced grant HYPXIMMUMO (ERC-ADG-2015, no. 694812), Walloon Region of Belgium through the SPW - DG Economie, Emploi, Recherche, its implementing body for regional research and innovation. The authors also acknowledge financial support from the EUROSTARS grant COMPACT (12053) and from Dutch Cancer Society (KWF grant number 8025) and the Cancer Society Auckland Northland, New Zealand (CSAN).

The costs of publication of this article were defrayed in part by the payment of page charges. This article must therefore be hereby marked *advertisement* in accordance with 18 U.S.C. Section 1734 solely to indicate this fact.

Received May 5, 2021; revised July 23, 2021; accepted September 30, 2021; published first October 8, 2021.

References

- Hockel M, Vaupel P. Tumor hypoxia: definitions and current clinical, biologic, and molecular aspects. *J Natl Cancer Inst* 2001;93:266–76.
- Vaupel P, Mayer A. Hypoxia in cancer: significance and impact on clinical outcome. *Cancer Metastasis Rev* 2007;26:225–39.
- Spiegelberg L, Houben R, Niemans R, de Ruyscher D, Yaromina A, Theys J, et al. Hypoxia-activated prodrugs and (lack of) clinical progress: The need for hypoxia-based biomarker patient selection in phase III clinical trials. *Clin Transl Radiat Oncol* 2019;15:62–9.
- Wilson WR, Hay MP. Targeting hypoxia in cancer therapy. *Nat Rev Cancer* 2011;11:393–410.
- Phillips RM. Targeting the hypoxic fraction of tumours using hypoxia-activated prodrugs. *Cancer Chemother Pharmacol* 2016;77:441–57.
- Guise CP, Mowday AM, Ashoorzadeh A, Yuan R, Lin W-H, Wu D-H, et al. Bioreductive prodrugs as cancer therapeutics: targeting tumor hypoxia. *Chin J Cancer* 2014;33:80–6.
- Sun JD, Liu Q, Wang J, Ahluwalia D, Ferraro D, Wang Y, et al. Selective tumor hypoxia targeting by hypoxia-activated prodrug TH-302 inhibits tumor growth in preclinical models of cancer. *Clin Cancer Res* 2012;18:758–70.
- Sun JD, Ahluwalia D, Liu Q, Li W, Wang Y, Meng F, et al. Combination treatment with hypoxia-activated prodrug evofosfamide (TH-302) and mTOR inhibitors results in enhanced antitumor efficacy in preclinical renal cell carcinoma models. *Am J Cancer Res* 2015;5:2139–55.
- Peeters SG, Zegers CM, Biemans R, Lieuwes NG, van Stiphout RG, Yaromina A, et al. TH-302 in combination with radiotherapy enhances the therapeutic outcome and is associated with pretreatment [18F]HX4 hypoxia PET imaging. *Clin Cancer Res* 2015;21:2984–92.
- Yaromina A, Granzier M, Biemans R, Lieuwes N, van Elmpt W, Shakinin G, et al. A novel concept for tumour targeting with radiation: inverse dose-painting or targeting the “Low Drug Uptake Volume”. *Radiother Oncol* 2017;124:513–20.
- Ganjoo KN, Cranmer LD, Butrynski JE, Rushing D, Adkins D, Okuno SH, et al. A phase I study of the safety and pharmacokinetics of the hypoxia-activated prodrug TH-302 in combination with doxorubicin in patients with advanced soft tissue sarcoma. *Oncology* 2011;80:50–6.
- Borad MJ, Reddy SG, Bahary N, Uronis HE, Sigal D, Cohn AL, et al. Randomized phase II trial of gemcitabine plus TH-302 versus gemcitabine in patients with advanced pancreatic cancer. *J Clin Oncol* 2015;33:1475–81.

13. Van Cutsem E, Lenz H-J, Furuse J, Tabernero J, Heinemann V, Ioka T, et al. MAESTRO: a randomized, double-blind phase III study of evofosfamide (Evo) in combination with gemcitabine (Gem) in previously untreated patients (pts) with metastatic or locally advanced unresectable pancreatic ductal adenocarcinoma (PDAC). *J Clin Oncol* 2016;34:4007.
14. Tap WD, Papai Z, Van Tine BA, Attia S, Ganjoo KN, Jones RL, et al. Doxorubicin plus evofosfamide versus doxorubicin alone in locally advanced, unresectable or metastatic soft-tissue sarcoma (TH CR-406/SARC021): an international, multicentre, open-label, randomised phase 3 trial. *Lancet Oncol* 2017;18:1089–103.
15. Higgins JP, Sarapa N, Kim J, Poma E. Unexpected pharmacokinetics of evofosfamide observed in phase III MAESTRO study. *J Clin Oncol* 2018;36:2568.
16. Millis KK, Colvin ME, Shulmanroskes EM, Ludeman SM, Colvin OM, Gamcsik MP. Comparison of the protonation of isophosphoramidate mustard and phosphoramidate mustard. *J Med Chem* 1995;38:2166–75.
17. Hong CR, Wilson WR, Hicks KO. An Intratumor Pharmacokinetic/Pharmacodynamic model for the hypoxia-activated prodrug evofosfamide (TH-302): monotherapy activity is not dependent on a bystander effect. *Neoplasia* 2019;21:159–71.
18. Patterson AV, Ferry DM, Edmunds SJ, Gu Y, Singleton RS, Patel K, et al. Mechanism of action and preclinical antitumor activity of the novel hypoxia-activated DNA cross-linking agent PR-104. *Clin Cancer Res* 2007;13:3922–32.
19. Abbattista MR, Jamieson SM, Gu Y, Nickel JE, Pullen SM, Patterson AV, et al. Pre-clinical activity of PR-104 as monotherapy and in combination with sorafenib in hepatocellular carcinoma. *Cancer Biol Ther* 2015;16:610–22.
20. Hunter FW, Hsu HL, Su J, Pullen SM, Wilson WR, Wang J. Dual targeting of hypoxia and homologous recombination repair dysfunction in triple-negative breast cancer. *Mol Cancer Ther* 2014;13:2501–14.
21. Jameson MB, Rischin D, Pegram M, Gutheil J, Patterson AV, Denny WA, et al. A phase I trial of PR-104, a nitrogen mustard prodrug activated by both hypoxia and aldo-keto reductase 1C3, in patients with solid tumors. *Cancer Chemother Pharmacol* 2010;65:791–801.
22. McKeage MJ, Gu Y, Wilson WR, Hill A, Amies K, Melink TJ, et al. A phase I trial of PR-104, a pre-prodrug of the bioreductive prodrug PR-104A, given weekly to solid tumour patients. *BMC Cancer* 2011;11:432.
23. Guise CP, Abbattista MR, Singleton RS, Holford SD, Connolly J, Dachs GU, et al. The bioreductive prodrug PR-104A is activated under aerobic conditions by human aldo-keto reductase 1C3. *Cancer Res* 2010;70:1573–84.
24. Birtwistle J, Hayden RE, Khanim FL, Green RM, Pearce C, Davies NJ, et al. The aldo-keto reductase AKR1C3 contributes to 7,12-dimethylbenz(a)anthracene-3,4-dihydrodiol mediated oxidative DNA damage in myeloid cells: implications for leukemogenesis. *Mutat Res* 2009;662:67–74.
25. Konopleva M, Thall PF, Yi CA, Borthakur G, Covelev A, Bueso-Ramos C, et al. Phase I/II study of the hypoxia-activated prodrug PR104 in refractory/relapsed acute myeloid leukemia and acute lymphoblastic leukemia. *Haematologica* 2015;100:927–34.
26. Patel K, Choy SS, Hicks KO, Melink TJ, Holford NH, Wilson WR. A combined pharmacokinetic model for the hypoxia-targeted prodrug PR-104A in humans, dogs, rats and mice predicts species differences in clearance and toxicity. *Cancer Chemother Pharmacol* 2011;67:1145–55.
27. Smail JB, Patterson AV, Ashoorzadeh A, Guise CP, Mowday AM, Ackerley DF, et al. Novel prodrugs and methods of use thereof. *PCT Int. Appl*; 2014, WO2014031012A1.
28. Smail JB, Patterson AV, Ashoorzadeh A, Guise CP, Mowday AM, Ackerley DF, et al. Prodrugs and methods of use thereof. *U.S. Pat. Appl. Publ.*; 2018, US 20180148463 A1.
29. Heyerick A, Deschoemaeker S, Thiollay S, Tersago D, Lambin P. Prodrugs and medical uses thereof. *WO* 2019229195 A1.
30. Gu Y, Atwell GJ, Wilson WR. Metabolism and excretion of the novel bioreductive prodrug PR-104 in mice, rats, dogs, and humans. *Drug Metab Dispos* 2010;38:498–508.
31. Gu Y, Tingle MD, Wilson WR. Glucuronidation of anticancer prodrug PR-104A: species differences, identification of human UDP-glucuronosyltransferases, and implications for therapy. *J Pharmacol Exp Ther* 2011;337:692–702.
32. Atwell GJ, Denny WA. Synthesis of 3H- and 2H4-labelled versions of the hypoxia-activated pre-prodrug 2-[(2-bromoethyl)-2,4-dinitro-6-[[[2-(phosphonoxy)ethyl]amino]carbonyl]anilino]ethyl methanesulfonate (PR-104). *J Label Compd Radiopharm* 2007;50:7–12.
33. Yang S, Atwell G, Denny W. Synthesis of asymmetric halomesylate mustards with aziridineethanol/alkali metal halides: application to an improved synthesis of the hypoxia prodrug PR-104. *Tetrahedron* 2007;63:5470–6.
34. Anderson RF, Yadav P, Patel D, Reynisson J, Tipparaju SR, Guise CP, et al. Characterisation of radicals formed by the triazine 1,4-dioxide hypoxia-activated prodrug, SN30000. *Org Biomol Chem* 2014;12:3386–92.
35. Guise CP, Abbattista MR, Tipparaju SR, Lambie NK, Su J, Li D, et al. Diflavin oxidoreductases activate the bioreductive prodrug PR-104A under hypoxia. *Mol Pharmacol* 2012;81:31–40.
36. Wilson WR, Hicks KO, Pullen SM, Ferry DM, Helsby NA, Patterson AV. Bystander effects of bioreductive drugs: potential for exploiting pathological tumor hypoxia with dinitrobenzamide mustards. *Radiat Res* 2007;167:625–36.
37. Yahyanejad S, van Hoof SJ, Theys J, Barbeau LM, Granton PV, Paesmans K, et al. An image guided small animal radiation therapy platform (SmART) to monitor glioblastoma progression and therapy response. *Radiother Oncol* 2015;116:467–72.
38. Hicks KO, Myint H, Patterson AV, Pruijn FB, Siim BG, Patel K, et al. Oxygen dependence and extravascular transport of hypoxia-activated prodrugs: comparison of the dinitrobenzamide mustard PR-104A and tirapazamine. *Int J Radiat Oncol Biol Phys* 2007;69:560–71.
39. Meng F, Evans JW, Bhupathi D, Banica M, Lan L, Lorente G, et al. Molecular and cellular pharmacology of the hypoxia-activated prodrug TH-302. *Mol Cancer Ther* 2012;11:740–51.
40. Langhans SA. Three-dimensional in vitro cell culture models in drug discovery and drug repositioning. *Front Pharmacol* 2018;9:6.
41. Nair AB, Jacob S. A simple practice guide for dose conversion between animals and human. *J Basic Clin Pharm* 2016;7:27–31.
42. Hunter FW, Wouters BG, Wilson WR. Hypoxia-activated prodrugs: paths forward in the era of personalised medicine. *Br J Cancer* 2016;114:1071–7.
43. Guise CP, Wang AT, Theil A, Bridewell DJ, Wilson WR, Patterson AV. Identification of human reductases that activate the dinitrobenzamide mustard prodrug PR-104A: a role for NADPH:cytochrome P450 oxidoreductase under hypoxia. *Biochem Pharmacol* 2007;74:810–20.
44. Hunter FW, Young RJ, Shalev Z, Vellanki RN, Wang J, Gu Y, et al. Identification of P450 oxidoreductase as a major determinant of sensitivity to hypoxia-activated prodrugs. *Cancer Res* 2015;75:4211–23.
45. Gu Y, Patterson AV, Atwell GJ, Chernikova SB, Brown JM, Thompson LH, et al. Roles of DNA repair and reductase activity in the cytotoxicity of the hypoxia-activated dinitrobenzamide mustard PR-104A. *Mol Cancer Ther* 2009;8:1714–23.
46. Deans AJ, West SC. DNA interstrand crosslink repair and cancer. *Nat Rev Cancer* 2011;11:467–80.
47. Hamis S, Kohandel M, Dubois LJ, Yaromina A, Lambin P, Powathil GG. Combining hypoxia-activated prodrugs and radiotherapy in silico: Impact of treatment scheduling and the intra-tumoural oxygen landscape. *PLoS Comput Biol* 2020;16:e1008041.